ADVANCED SUSTAINABLE SYSTEMS
www.advsustainsys.com

Avocado Pruning Residues for the Formulation of Bio-Based Polyethylene/Fiber-Based Biocomposites for Sustainable Food Packaging

Ramón Morcillo-Martín, Quim Tarrés, Roberto J. Aguado, Eduardo Espinosa,* Marc Delgado-Aguilar, and Alejandro Rodríguez*

The extensive use of non-biodegradable bioplastics and fossil-based plastics in food packaging presents a significant environmental challenge. Consequently, there has been a growing interest in exploring agricultural biomass as a potential source for formulating biocomposites for packaging due to the substantial amount of lignocellulosic residue generated. This study explores the utilization of avocado pruning residue (APR) for isolating lignocellulose fibers and their application as replacement and reinforcement material for bio-based polyethylene (BioPE) composites. The results obtained reveal that a concentration of 9% (w/w) of maleic anhydride-grafted-polyethylene (MAPE) shows the most effective fiber–polymer interaction, resulting in a significant improvement of 25.47% in the mechanical properties. Biocomposites with varying fiber concentrations, ranging from 10% to 40% (w/w), are prepared and assessed for their macro- and micromechanical properties. The results demonstrate a substantial 49% increase in tensile strength and a remarkable 325% enhancement in Young's modulus for biocomposites containing 40% (w/w) fiber content. Furthermore, micromechanical analysis provides insights into the intrinsic strength and modulus of avocado fibers, with values of ≈437 MPa and 33 GPa, respectively. This research contributes to the development of sustainable and eco-friendly alternatives for food packaging, reducing the reliance on fossil-based plastics, and promoting the utilization of agricultural waste.

1. Introduction

Plastic ranks as the most commonly used polymer in rigid food packaging due to its exceptional versatility, fluidity, moldability, heat stability, and ease of scalability in the production chain.[1] Over the past five decades, its production has experienced a surge, increasing from 15 million tons in 1964 to ≈391 million tons in 2021, with expectations of doubling over the next 15 years.[2,3] In Europe, more than 20 billion kilograms of plastic are used for packaging, with ≈8.2 billion kilograms dedicated to food products. However, despite the undeniable advantages offered by plastic materials, their excessive usage has led to severe social and economic consequences. Given their limited recyclability, short lifespan, and massive production quantities, plastic packaging materials often end up discarded within a year of their production. This has resulted in a significant solid waste problem, exacerbated by inadequate waste management systems that fail to effectively collect and dispose of plastic materials, ultimately leading to their accumulation in aquatic environments.[4] Annually, a minimum of 25 million tons of plastic leaks into the ocean, equivalent to dumping the contents of one garbage truck into the ocean every minute. If no action is taken, this rate is expected to increase to two per minute by 2030 and four per minute by 2050.[2]

Addressing this problem requires a two-pronged approach. First, the creation of policies and regulatory frameworks that genuinely promote sustainable development by reducing the use of petroleum-based materials, such as plastics. Furthermore, this needs to be coupled with the development of efficient systems for collection, separation, and waste management that ensure a suitable end-of-life depending on the material's ability to biodegrade, presence of multiple layers and/or additives, possible contamination with food waste, market share, processing structure, and available collection sites.[5,6] Based on these criteria the selection of the most suitable end-of-life scenario (recycling, biodegradation, composting, incineration, or landfilling) should be addressed. Second, the implementation of new technical solutions

R. Morcillo-Martín, E. Espinosa, A. Rodríguez
BioPren Group
Chemical Engineering Department
Instituto Químico para la Energía y el Medioambiente (IQUEMA)
Universidad de Córdoba
Córdoba 14014, Spain
E-mail: eduardo.espinosa@uco.es
Q. Tarrés, R. J. Aguado, M. Delgado-Aguilar
LEPAMAP-PRODIS Research Group
University of Girona
C/ Maria Aurèlia Capmany, Girona 61-17003, Spain
E-mail: joaquimagusti.tarres@udg.edu

The ORCID identification number(s) for the author(s) of this article can be found under https://doi.org/10.1002/adsu.202300600

DOI: 10.1002/adsu.202300600

that replace the use of the aforementioned materials, with a focus on biobased, biodegradable, and compostable polymers. In recent years, more restrictive regulations have been adopted, such as the EU Directive 2019/904, primarily aimed at reducing the use of single-use plastics (SUPs) in various products and the EC 94/62 and posterior amendments (2018/852) which lays down measures to prevent the production of packaging waste, promoting a more circular economy.[7,8] On the other hand, in the quest for alternative materials to replace fossil-based polymers, EU´s strategic autonomy relies on the use of sustainably sourced biomass, in particular organic waste and residues, over primary biomass.[9] The use of these resources is crucial in promoting genuine independence from oil, thereby, enhancing the economic prospects of regions through the agricultural industry's economic cycle. Moreover, lignocellulosic biomass (LB) has gained recognition as a promising renewable feedstock for biopolymer production.[10] In the literature, three different strategies have been employed to valorize LB for rigid packaging production: bioplastics, molded fiber products, and biocomposite materials. The first strategy involves substituting fossil-based sources with LB-derived bioplastics. One example of LB-derived bioplastic is the bio-polyethylene (BioPE). The BioPE production involves dehydrating bioethanol into ethylene and subjecting it to a complex chemical process to obtain BioPE as final product.[11] As a second strategy, molded fiber and its products have garnered attention due to their biodegradability, renewability, and recyclability,[12] though their mechanical and barrier properties are not always suitable for food packaging requirements. The other alternative is the production of biocomposite materials where lignocellulosic-derived components are a major element in the composition, increasing the biodegradability and sustainability of the final packaging material. Among the three predominant components of LB (cellulose, hemicellulose, and lignin), lignocellulosic fibers have been proposed as partial substitute materials for thermoplastic polymers. Their use alone or in conjunction with fiber–polymer compatibilizing agents, such as maleic anhydride, offers certain advantages over the use of bioplastics or biopolymers alone, including mechanical reinforcement of the thermoplastic polymer, lower cost, and reduced environmental impact through circular waste utilization. Furthermore, due to their higher aspect ratio compared to lignocellulosic particles, lignocellulosic fibers have been extensively studied for their potential as components in biocomposites.[13]

The sources of biomass for lignocellulosic fiber isolation are diverse, making the agricultural sector a significant contributor to its generation. Notably, Andalucía (Spain's southern region) boasts an extensive agricultural expanse of ≈3.7 million hectares.[14] Furthermore, in recent years, there has been a remarkable upsurge in fruit tree cultivation, particularly in the avocado crop, driven by its growing popularity as a nutritious food choice. Specifically, in 2022/2023 season, the production of avocado fruit in Andalucía reached a production value of 78.38 thousand tons, accounting for almost 74% of national production. The need for a tropical climate for the development of these fruits concentrates the production in Malaga and Granada regions, constituting 46.3% and 16.3% of the total nationwide, respectively.[15] This substantial production inevitably results in the generation of a significant volume of pruning residues from avocado trees. Regrettably, in many cases, these valuable residues are utilized for agricultural amendments or combusted for energy generation, underestimating their potential to create added value.[16] The abundant availability of avocado pruning residue (APR), combined with the imperative need to reduce plastic consumption, highlights the critical importance of integrating these residual materials within a circular bioeconomy framework. Although there are studies demonstrating the suitability of avocado pruning to produce cellulosic pulps comparable to those obtained from hardwood feedstocks,[17] it is worth noting that, to the best of our knowledge, there are currently no studies that assess the potential of APR as a substitute material for plastics in rigid food packaging. Exploring the viability of utilizing APR as an alternative to partial substitution of plastics in rigid food packaging presents an exciting avenue for research and innovation, aligning with the principles of sustainability and waste reduction. With the accomplishment of this research, progress is being made toward a more environmentally friendly and resource-efficient approach to food packaging, taking advantage of the untapped potential of APR.

To explore the development of alternative food packaging materials that can reduce the use of plastic polymers, the isolation of lignocellulose fibers from APR (which will be referred as APF from now on) as a reinforcing material for non-biodegradable bioplastic matrices, specifically bio-polyethylene (BioPE) was successfully achieved. This study also focused on optimizing the concentration of MAPE, selecting a concentration of 9% (w/w) (fiber weight) to produce BioPE-APF biocomposites ranging from 10 to 40% (w/w). To gain a better understanding of how the intrinsic properties of the phases affect the macro-properties of the composite, the micromechanical aspects of BioPE-based composites were evaluated.

2. Experimental Section

2.1. Materials

The avocado pruning residue (APR) used in this work was provided by an independent farmer from Salobreña (Spain). The APR was dried at room temperature to a moisture content below 10% (w/w). Branches from 10 to 100 cm were selected and grounded to a size of 2–5 cm. For chemical analysis, samples were prepared according to TAPPI standard T-264. The reagents used in this work were: acetic acid (ACS reagent ≥99.7%); hydrochloric acid (Sigma–Aldrich, 37%); sodium chlorite (Sigma–Aldrich, >99%); Sodium hydroxide (Sigma–Aldrich, >99%); maleic anhydride-grafted-polyethylene (MAPE) with a maleic-anhydride substitution of 0.9% (Fusabond MB100D). Biopolyethylene (BioPE) injection grade SHA7260 was supplied by Braskem (Sao Paulo, Brazil) (molecular weight of 61.9 g mol^{-1}).

2.2. Methods

2.2.1. APR Fiber Production and Characterization

To produce lignocellulose fibers from APR, the procedure described by Espinosa et al.,[18] was followed with some modifications. The APR was subjected to an alkaline treatment in a rotary reactor under the following operating conditions: 90 min, 170 °C,

22% sodium hydroxide (NaOH) based on dry weight basis (dwb), maintaining a liquid-to-solid ratio (l:s) of 5:1. After the pulping process, the solid fraction underwent a refining process using a Sprout–Bauer refiner obtaining the avocado pruning residue cellulosic pulp (APF). The chemical composition of APR and APF was analyzed by the following standards: extractives (Tappi T-204), ashes (Tappi T-211), lignin (Tappi T-222), holocellulose (Tappi T-9wd75), and α-cellulose (Tappi T-429). To analyze the fiber morphology before and after the production of composites, the fibers were extracted from the composite material after the injection molding process. The extraction of fibers was performed using a Soxhlet apparatus with toluene as the solvent for BioPE. The obtained APF and those extracted from the composite material were then analyzed using a MORFI laboratory equipment (Techpap, France). For this analysis, a fiber suspension with a concentration of 25 mg L^{-1} was prepared and four measurements (30 000 fibers $test^{-1}$) were realized. Through this analysis, the average length and diameter of the fibers were determined, along with their distribution.

2.2.2. Compounding and Processing of the BioPE-APF Biocomposites

The production of BioPE-APF biocomposites were produced according to Tarrés et al.[19] Briefly, the APF were incorporated into the BioPE (bio-polyethylene) matrix along with the MAPE (maleic anhydride grafted polyethylene) coupling agent using a Gelimat intensive kinetic mixer (Dusatec, NJ, USA). The compounding process was carried out for 2 min at 2700 rpm to reach the melting temperature, and the mixture was discharged when the temperature was 210 °C. First, we study different percentages of MAPE coupling agent: 3%, 6%, 9%, and 12% (w/w) based on dry fiber weight for compounds containing 20% (w/w) of APF. The obtained biocomposites were named BioPE-3MAPE, BioPE-6MAPE, BioPE-9MAPE, and BioPE-12MAPE. Once the optimal MAPE addition percentage was determined (9%, w/w), it was used for the formulation of composites containing 10% to 40% (w/w) APF, which were named BioPE-10APF, BioPE-20APF, BioPE-30APF, and BioPE-40APF. Sample codification and composition are presented in **Table 1**. The resulting blends were ground with knives mill and dried at 80 °C until they were ready for use in the injection molding process to produce samples. Standard composite dog-bone shaped specimens were produced according to ASTM D638 using an Arburg 220 M 350-90U injection machine (Lossburg, Germany). The injection process involved a temperature profile of 185, 190, 195, 195, and 190 °C, with a first pressure of 120 kg cm^{-2} and a second pressure of 37.5 kg cm^{-2}.

2.2.3. Mechanical Characterization

The specimens were stored in a conditioning chamber at 23 °C and 50% relative humidity for 48 h, following the guidelines of the ASTM D638 standard. Composites were tested using a dynamometer DTC-10 provided by IDMtest (San Sebastián, Spain), equipped with a 5 kN load cell, and operated at a crosshead speed of 2 mm min^{-1}. Tensile properties were analyzed in accordance with the ASTM D638 standard. The reported results represent the average of at least five samples. The density of the different blends was calculated using a pycnometer, and the specific mechanical properties were calculated.

Table 1. Sample codification and composition of the different biocomposites.

Sample code	BioPE [%, w/w]	Fibers [%, w/w]	MAPE compatibilizer [%, w/w based on dry fiber weight]
BioPE	100	–	–
BioPE-0MAPE	80	20	–
BioPE-3MAPE	77		3
BioPE-6MAPE	74		6
BioPE-9MAPE	71		9
BioPE-12MAPE	68		12
BioPE-10APF	81	10	9
BioPE-20APF	71	20	
BioPE-30APF	61	30	
BioPE-40APF	51	40	

2.2.4. Scanning Electron Microscopy (SEM), Melt Flow Index (MFI), Thermogravimetric Analysis (TGA), Differential Scanning Calorimetry (DSC), and Water Uptake

To further study the developed materials, morphological, and thermal analysis of the different biocomposites were performed. The morphologies of fractured samples were observed under a scanning electron microscope (Zeiss DSM 960A SEM instrument) to examine the fiber-matrix compatibility at the interface as well as the external appearance of the composites. Prior to measurement, the samples were sputter-coated with gold and observed at an accelerated voltage of 7 kV.

The melt flow index (MFI) test was conducted using a CEAST plastometer from (Pianezza, Italy). The plastometer is fitted with two thermal resistors that heat a capillary. In this specific test, the temperature was set at 200 °C, using a weight of 2.16 kg. The test measured the quantity of material melted and discharged within a 10-min period, following the guidelines outlined in the ISO 1133 standard.

Thermogravimetric analysis (TGA) was performed using a Metler Toledo SDTA851 equipment (Mettler Toledo, L'Hospitalet de Llobregat, Spain). The APF and biocomposite samples were subjected to a heating process from 30 to 700 °C at a rate of 10 °C min^{-1}. The test was conducted in an inert atmosphere with a nitrogen flow rate of 40 mL min^{-1}.

Differential scanning calorimetry (DSC) was conducted using a Mettler Toledo DSC822e thermal analyzer (Mettler Toledo, L'Hospitalet de Llobregat, Spain) to assess the impact of the incorporated APF on the thermal transitions and crystallinity degree of the matrix according to ASTM E1269.01 standard specifications. The samples were initially heated from 30 to 220 °C during the first heating scan to eliminate their thermal history. Subsequently, cooling was performed, and the samples were reheated within the same temperature range. All scans were carried out at a heating or cooling rate of 10 °C min^{-1} under a nitrogen

Table 2. Chemical composition of the APW and the APF.

Sample	Extractables [%]	Lignin [%]	Hemicelluloses [%]	α-cellulose [%]	Ashes [%]
APW	18.37[a] ± 1.61	21.09[a] ± 1.9	22.14[a] ± 1.29	28.85[a] ± 2.71	5.96[a] ± 0.12
APF	7.47[b] ± 2.84	7.56[b] ± 3.86	18.37[a] ± 0.08	63.12[b] ± 5.19	6.72[b] ± 0.05

atmosphere with a flow rate of 40 mL min^{-1}. The crystallinity level (X_c) was determined from the second heating DSC traces according to Equation 1:

$$X_c\,(\%) = \frac{\Delta H_f}{\Delta H_{ref}}\,\frac{100}{x} \tag{1}$$

where ΔH_f is the experimental enthalpy of fusion, ΔH_{ref} is the theoretical enthalpy of fusion of fully crystalline polyethylene (293 J g^{-1}),[20] and x is the weight fraction of BioPE in the composites.

Since the intended application of these materials is food packaging, the 24 h water uptake of the different biocomposites was evaluated following ASTM-D570 standard. The percentage of water uptake was calculated from Equation 2:

$$\text{Water uptake}\,(\%) = \frac{W_1 - W_0}{W_0} \times 100 \tag{2}$$

where W_1 and W_0 stands for the weight of the composite after and before the 24 h immersion, respectively.

2.2.5. Statistical Analysis

Mean and standard deviation values were reported based on a minimum of five replicates of each sample ($n = 5$). Analysis of variance (ANOVA) was utilized to determine statistically significant differences between APW and APF compositions as well as the characterization of BioPE-APF biocomposites. Tukey posthoc analysis was conducted to evaluate differences among mean values. The statistical analysis was performed using IBM SPSS Statistics version 25 software (IBM, USA). Significance was defined at $p < 0.05$.

3. Results and Discussion

3.1. Chemical and Morphological Characterization of the APR and APF

The ability of the fibers to bond with the polymeric matrix is influenced by various factors, the morphological characteristics of the fibers and their chemical composition are particularly significant.[21] The results of the chemical characterization of APR and APF, as well as the fiber morphological analysis, can be found in **Table 2** and Figure S1 (Supporting Information), respectively. APR exhibits the typical chemical composition of a lignocellulosic material, with cellulose (28.85%), hemicellulose (22.14%), and lignin (21.09%) as major fractions. This composition present higher potential to those observed for other avocado by-products, such as seeds and peels, characterized by a low cellulose content and a high presence of extractable constituents.[22] Following the alkaline pulping process the cellulosic fraction significantly increased ($p < 0.05$) by ≈119%, demonstrating the effectiveness of the selected pulping conditions. The yield of this process was calculated by a gravimetric method, obtaining a mean value of 52.2 ± 2.7%. In contrast, the lignin content decreased significantly, primarily due to its high solubility in alkaline media. The chemical composition of the fiber plays a crucial role in its suitability for reinforcing thermoplastic matrices. Cellulose is considered as the principal structural element within the fiber, imparting strength, rigidity, and overall structural stability.[23] Hemicellulose is closely associated with lignin, forming lignin–carbohydrate complexes (LCC) where lignin acts as a compacting agent. The presence of inter- and/or intramolecular hydrogen bonds in this structure and with cellulose molecules, limits the fiber's interaction with other polymers.[24] However, complete removal of these two components does result in a slight reduction of tensile stress, as lignin and hemicellulose function as natural binders for micro-fibrils on the natural fiber.[25] Furthermore, the compatibility between cellulose and other hydrophobic biopolymers could be enhanced by the amphiphilic lignin with polar phenolic OH and non-polar hydrocarbon groups.[26] Zhu et al.[27] have previously conducted research on the impact of these three primary fiber constituents in enhancing biopolymer reinforcement. They concluded that the best composition of sisal fibers to reinforce PLA matrix was 71.4% cellulose, 16.6% hemicellulose, and 12% lignin, closely resembling the results obtained for APF in our study. Focusing on avocado fibers morphology it shows lengths and diameters comparable to those found in other short fibers derived from agricultural residues used in reinforcing polymeric matrices, such as rice straw, kenaf (core), coconut coir, or corn.[28] In summary, both the APF chemical composition and its morphological characteristics substantiate the rationale for utilizing this fiber in our study to enhance the performance of thermoplastic matrices.

3.2. Engineering Optimal Interfaces for APF-BioPE Biocomposites

The addition of MAPE had a significant impact on the mechanical properties of the composites (Table S1, Supporting Information).

Figure 1a clearly illustrates that increasing the amount of the coupling agent results in higher tensile strength and strain at break in the composites, indicating a significant advantage over uncoupled composites. Specifically, the tensile strength improved with the addition of MAPE up to 9%. However, further increases in MAPE content led to a decrease in the strength of the composites. Therefore, for subsequent formulations, a 9% MAPE content was chosen as the optimum (see Section 3.3). Similar trends have been reported in prior studies conducted by

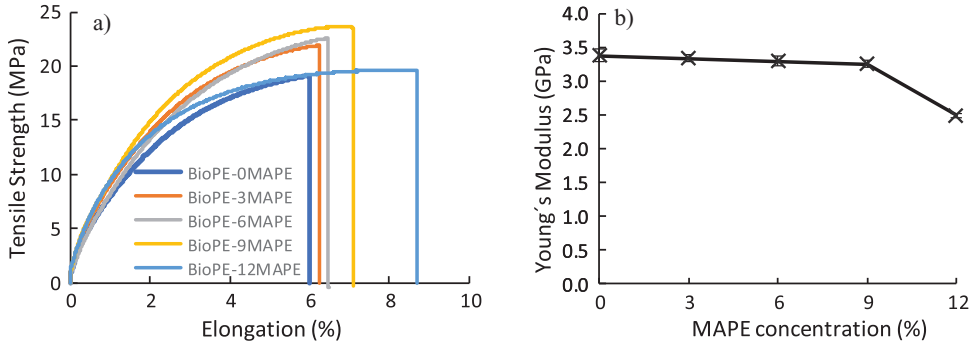

Figure 1. Results of the mechanical properties for a) Tensile Strength and b) Young´s Modulus for the different concentrations of MAPE for compounds containing 20% (w/w) APF.

Chen et al.[29] and Wang et al.,[30] where the addition of MAPE concentrations above 6% resulted in decreased tensile strength in composite materials with a 20% of fiber reinforcement. The increase in the strength of the composite materials due to the addition of the coupling agent can be attributed to two key mechanisms extensively discussed in the literature,[31] as presented in **Figure 2**. First, the coupling agent facilitates the formation of covalent bonds in the form of esters (C—O) between the maleic anhydride molecule in MAPE and the hydroxyl groups on the surface of the lignocellulose fibers. This chemical reaction establishes a stronger connection between the fibers and the matrix, thus creating a more intimate interface (see Section 3.4). Moreover, Lu et al.[32] propose a broader interfacial bonding based on hydrogen bonding, van der Waal's forces and physical interactions. Second, the polyethylene chains present in MAPE disperse and intertwine with the polymeric matrix, leading to random entanglements. However, these mechanisms are effective only up to a certain concentration of MAPE. Beyond this threshold, as observed in BioPE-12MAPE samples, the material properties are compromised. At high concentrations of MAPE, the entirety of the fiber is bound, resulting in an excess of MAPE in the composites. This excess contributes to lower stiffness and tensile strength in the composite caused by two different phenomena. First, the addition of high contents of coupling agent results in the increase of short-chain polyethylene present in MAPE. Since the tensile strength of the compatibilizer is roughly similar to BioPE,[30,33] the excess of coupling agent acts as the matrix, lowering the overall strength. Second, once the entirety of the hydroxyl groups present in the fiber are saturated, the MAPE molecules tend to self-react and self-entangle, which adversely affects the interface.[19,34] This increase in the quantity of short-chain polyethylene and the self-interaction of MAPE leads to a decrease in the intrinsic properties of the material.

The tangent angle of the stress–strain curves at the origin, also known as the Young´s modulus, is depicted in Figure 1b. As shown, the samples exhibited similar values, with the exception of the 12% sample, which displayed a significant decrease in Young's modulus (see Table S2, Supporting Information). Previous research suggests that the interface strength has a limited impact on the Young's modulus of a material.[19,35,36] This find-

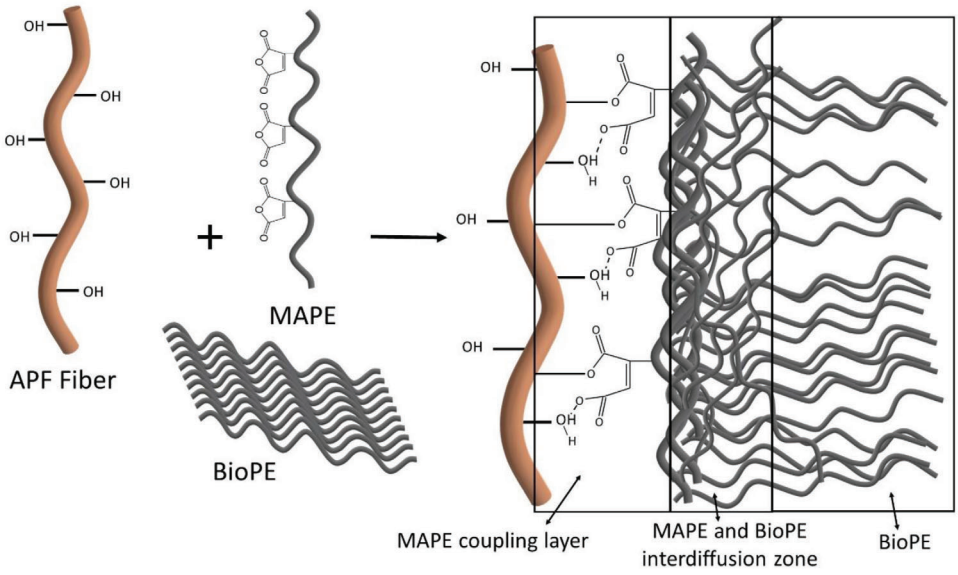

Figure 2. Interaction mechanism involving avocado fiber, MAPE coupling agent and the polymeric matrix (BioPE).

Table 3. Evolution of the tensile properties of the composites with different APF contents.

Samples	Density [g cm^{-3}]	σ_t^c [MPa]	E_t^c [GPa]	ε_t^c [%]	Specific σ_t^c [MPa cm^3 g^{-1}]	Specific E_t^c [GPa cm^3 g^{-1}]
APF	1.49 ± 0.04^a					
BioPE	0.94 ± 0.02^b	18.05 ± 0.11^a	1.06 ± 0.03^a	10.59 ± 0.06^a	19.16 ± 0.11^a	1.13 ± 0.03^a
BioPE-10APF	1.15 ± 0.03^c	16.61 ± 0.32^b	2.03 ± 0.03^b	9.14 ± 0.3^b	14.39 ± 0.32^b	1.76 ± 0.03^b
BioPE-20APF	1.2 ± 0.03^c	23.89 ± 0.58^c	3.33 ± 0.05^c	7.79 ± 0.49^c	19.86 ± 0.58^a	2.77 ± 0.05^c
BioPE-30APF	1.23 ± 0.11^c	24.45 ± 0.89^c	3.7 ± 0.08^d	5.21 ± 0.19^d	19.94 ± 0.89^a	3.02 ± 0.08^d
BioPE-40APF	1.22 ± 0.09^c	26.88 ± 0.49^d	4.5 ± 0.22^e	3.37 ± 0.53^e	21.97 ± 0.49^c	3.68 ± 0.22^e

ing remains consistent for the 3—9% MAPE samples. It is well-established that the failure of composite materials is typically attributed to the weakest phase among the matrix, reinforcement, and interface.[36] In most cases, the interface is considered the weakest phase as it facilitates the transfer of loads between the fiber and matrix. This load transfer involves converting matrix tensile loads into interface shear loads, which are subsequently converted into tensile loads within the reinforcement.[37] Therefore, the use of high concentrations of coupling agents, such as 12%, could result in a less rigid phase, ultimately reducing the stiffness of the blend and leading to a decline in Young's modulus.[38,39]

3.3. Biocomposite Mechanical Properties and Effect of APF Addition

After optimizing the MAPE concentration, the reinforcement capacity of the APF was examined using different concentrations ranging from 10% to 40% (w/w), with 9% selected as the optimal coupling agent concentration.

Table 3 presents the tensile strength (σ_t^c), Young's modulus (E_t^c), maximum strain at rupture (ε_t^c), and specific mechanical properties of the 10%–40% (w/w) APF reinforced BioPE composites. Incorporating APF into BioPE matrix had a substantial impact on the tensile properties of the biocomposites. For samples containing 20%–40% (w/w), the tensile strength increased by 32%, 36% and 49%, respectively, when compared to the matrix. However, a decrease in strength of ≈8% was observed for the 10% (w/w) composites in comparison to the matrix. This reduction suggests that at this concentration, the fibers are not uniform distributed on the matrix. The reinforcing effect of the fibers exhibited a linear trend for σ_t^c with an R^2 value of 0.9953 (see Figure S1, Supporting Information). These results indicate the presence of a strong interface between the fibers and the matrix. The consistent linear increase in tensile strength further suggests that the fibers are well dispersed within the matrix. The level of reinforcement achieved was significantly higher than that reported by Mohanty et al.,[40] and Carbonell-Verdú et al.[41] In their respective studies, the addition of 30% (w/w) untreated jute fiber and slate fiber to HDPE matrices improved the tensile strength by up to 31%, and 16% compared to the matrices, respectively. While σ_t^c showed a directly proportional relationship with the fiber content, an inverse relationship was observed for (ε_t^c). This indicates a decrease in the deformation at rupture of the material, which is a direct consequence of Hooke´s law.

The relationship between E_t^c and APF content illustrates the significant influence of these reinforcements on the stiffness of the composites. Increasing the fiber content from 10% to 40% (w/w) led to a remarkable improvement in modulus, with increases of 92%, 214%, 249%, and 325% compared to the BioPE matrix. These results are comparable to those reported for HDPE composites reinforced with glass fiber, where values of 3.1 and 4.4 GPa were obtained for composites containing 20% and 30% glass fiber, respectively.[42] Furthermore, existing literature suggests a linear relationship between E_t^c and the volume fraction of reinforcement, which was confirmed in this study (see Figure S2, Supporting Information), obtaining a linear regression coefficient of $R^2 = 0.9943$. The better results observed for E_t^c can be attributed to a great dispersion of fibers into the matrix, as well as the low impact of interface strength on the Young´s modulus of a short-fiber-reinforced composite.[43]

The strength-to-weight ratio is an important index when selecting materials for high-strength and lightweight applications, such as food packaging. Therefore, the densities of the different composite materials were used to calculate the specific mechanical properties, obtaining specific strength and modulus values. Overall, the specific σ_t^c and E_t^c values are lower than those obtained in the non-specific mechanical properties. This can be attributed to the relatively high density of the APF ($\rho = 1.49$ g cm^{-3}) compared to the BioPE matrix ($\rho = 0.94$ g cm^{-3}), which results in denser materials and consequently a decrease in mechanical performance. In particular, the specific σ_t^c remained similar for all blends except for the 10% and 40% (w/w) formulations, which were significantly below and above the matrix, respectively. On the other hand, the specific E_t^c showed a similar trend to that reported in the non-specific E_t^c. Although the specific properties did not show improvement compared to the BioPE until sufficient fiber was added, the materials demonstrated an ability to achieve mechanical performance per gram of material that was equal to or exceeded that of the BioPE matrix. This suggests the potential of APF for partial substitution of bioplastics, leading to material savings due to the low cost of the fibers compared to BioPE and the production of more biodegradable materials.

3.4. Morphology and Thermal Behavior of the Composites

Figure 3 presents SEM micrographs of various specimens. A comparison between the developed biocomposites and the BioPE polymeric matrix reveals a considerably more organized structure in BioPE (as depicted in Figure 3a). This can be partly attributed to the surface alignment of polymeric chains during

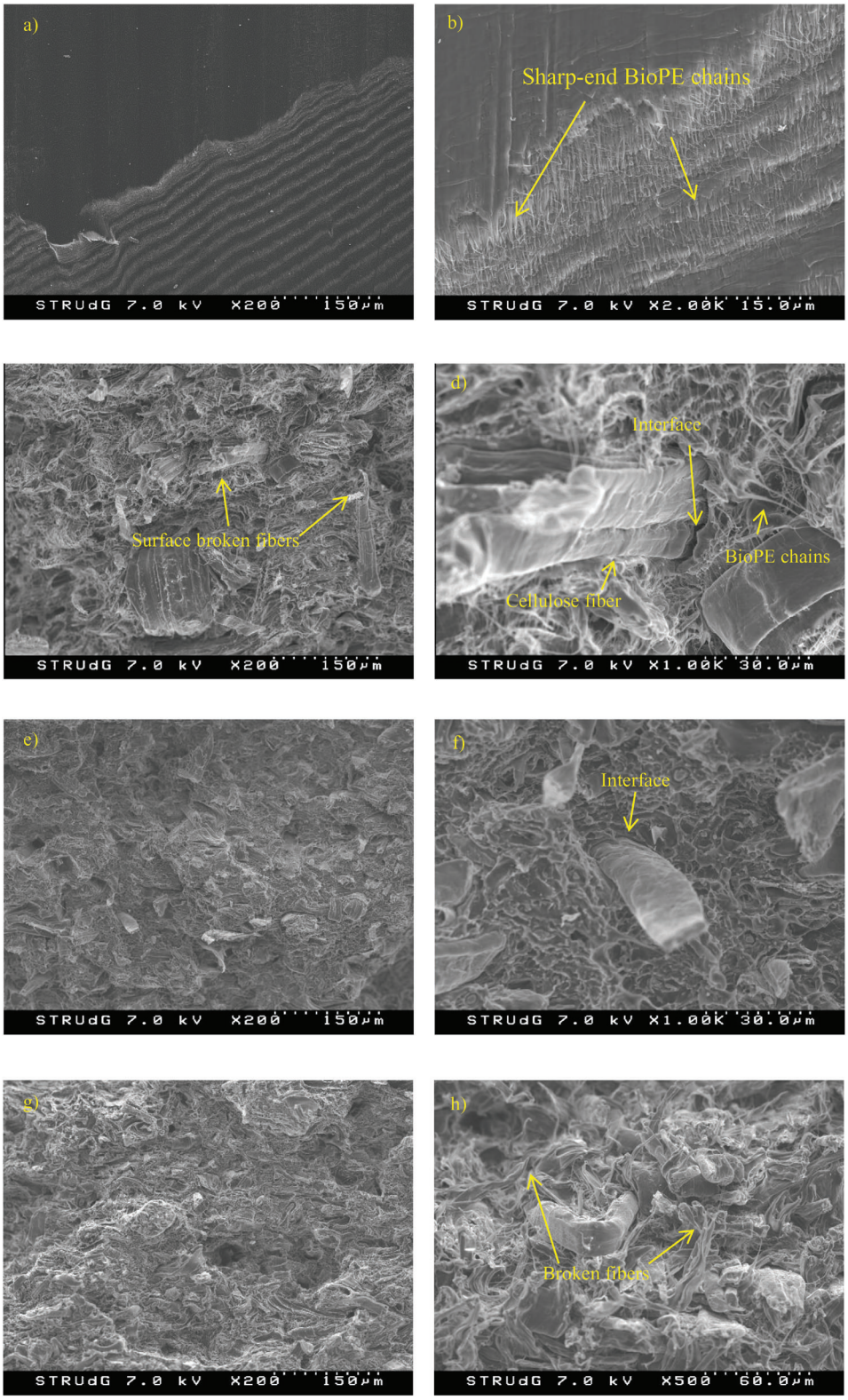

Figure 3. SEM micrographs of the surface and fractured sections of BioPE (Figure 3a,b), BioPE-0MAPE (Figure 3c,d), BioPE-20APF (Figure 3e,f), and BioPE-40APF (Figure 3 g,h), respectively.

the injection molding process, coupled with the relatively high crystallinity exhibited by HDPE.[44] However, the incorporation of lignocellulose fibers results in a heterogeneous blend, as evidenced by Figure 3b,d–f. Concerning the impact of MAPE on the fiber–polymer interaction, uncoupled samples (Figure 3d) exhibit a greater interface distance between the matrix and the fiber compared to coupled ones (Figure 3f). This observation confirms the expected results of the coupling agent, creating a stronger and denser structure (Figure 3e) with fewer voids than in uncoupled ones (Figure 3c). These observations align with the results obtained from the optimization of MAPE, with the coupled samples demonstrating a 20.4% higher tensile strength compared to the values observed in the uncoupled blend.

The MFI, TGA, DTG, and DSC results of the different selected samples are presented in Table S3 (Supporting Information). Studying the effect of temperature on the compounding and injection molding of the biocomposites is of particular interest since it can lead to the thermal degradation of the samples. Moreover, the thermal properties of the materials are of great concern, especially in the context of food packaging, where temperature fluctuations are anticipated. Table S3 (Supporting Information). displays the melt flow index (MFI), melting (*T*m), and crystallization (*T*c) temperatures, the enthalpy of fusion (ΔH_f), and the crystallinity index (χc) for BioPE and different biocomposites. The flowability of the composites was affected by the presence of MAPE and APF content. The non-thermoplastic behavior of the APF along with the enhanced interconnection with BioPE in coupled composites lead to lower shear rates, reducing 16 times the fluidity index when 40% APF was added to the biocomposites. The table reveals an increase in the *T*m of the virgin matrix by 4.4 °C with the incorporation of uncoupled APF. This increase is attributed to the interactions between fibers and between fibers and the polymer, resulting in a slight elevation of the melting point in uncoupled composites.[45] However, when MAPE was added to the biocomposites formulation, a reduction in the melting point was observed, approaching values similar to those of the matrix. This suggests improved fiber-matrix adhesion in the presence of MAPE. The addition of APF to the BioPE matrix produced a dilution effect, reducing the amount of melting energy required by up to 41.4% compared to pure BioPE. The crystallinity degree of BioPE was ≈63%, a value that closely corresponds to what has been reported in the literature.[46] Table S3 (Supporting Information) also showed that the composite samples exhibited a lower percentage crystallinity (*X*c) than the neat BioPE. The crystallinity reduction can be attributed to the dual role of cellulose fibers. On one hand, the nucleation effect of unmodified cellulose fibers through the generation of transcrystallinity has been documented in the literature.[47] However, simultaneously, the mobility of BioPE chains is constrained by the presence of cellulose fibers. Additionally, the cellulose fibers may act as barriers that influence the growth of crystals in the material. The incorporation of compatibilizers is noted to raise *X*c, primarily owing to the effective enhancement of interfacial interactions promoted by them. This effect of MAPE in promoting an increase in the crystallinity, has been previously reported by other authors and is associated with improved fiber adhesion to BioPE, which counteracts the inhibitory effect of APF on BioPE crystal formation.[48,49]

Turning to the decomposition temperatures and residual mass, noticeable differences were observed among the samples. The addition of APF to the BioPE matrix reduced the thermal degradation of the samples to ≈350 °C (**Figure 4**). This temperature confirms the adequate thermal stability of the samples for the mixing and injection molding process, where temperatures do not exceed 220 °C for compounding and 200 °C in the injection molding machine. Degradation of the BioPE matrix occurs in the temperature range of 385–515 °C, primarily involving the breaking of C—C bonds in the main polyethylene chain.[50] Introducing fibers into the HDPE matrix results in a reduced thermal stability of the composite, mainly due to the lower thermal stability of the fibers compared to HDPE, which accelerates the decomposition of BioPE within the composite.[51] While unfilled BioPE undergoes a single degradation stage, the addition of fibers clearly results in two distinct stages. The first stage occurs in the temperature range of 250–385 °C and corresponds to the degradation of the fibers.[52,53] The second main stage is observed between 430 and 520 °C, associated with the degradation of BioPE. Consequently, the composites exhibit intermediate thermal stability between that of the fibers and the matrix.[54,55]

In order to assess the suitability of the materials obtained for packaging foodstuffs that require storage at high relative humidity contents, as well as foods that could present leakages, the 24 h water uptake was measured. The results reported in **Figure 5** shows a direct proportional relationship between the fiber content in the biocomposites and the water uptake, obtaining a linear correlation coefficient of $R^2 = 0.923$, as shown in Figure S3 (Supporting Information). At low fiber concentrations the water uptake values were similar to those obtained for the hydrophobic BioPE, without reaching values above 0.3%. The fact that fibers are usually embedded in the thermoplastic matrix,[56] makes the surface of the composites waterproofed, reducing surface water absorption capacity. However, when increasing the fiber concentration, a higher number of free fibers (not embedded) are present, thus facilitating the swelling of the composite. This significant increase in the water affinity of fiber reinforced biocomposites has also been reported by multiple authors.[57–59] Despite the higher results in BioPE-30%APF and BioPE-40%APF samples, the water uptake was not higher than 11%.

3.5. Intrinsic Properties and Shear Stress Transfer

Composite materials are renowned for their exceptional strength, a property determined by three key factors: intrinsic matrix strength, intrinsic fiber strength, and interface strength. These elements are formally defined within the framework of the modified rule of mixtures equation (Equation 3), a widely accepted standard for characterizing composite strength.[60,61]

$$\sigma_t^C = f_c \times \sigma_t^F \times V^F + \left(1 - V^F\right) \times \sigma_t^{m^*} \quad (3)$$

The contribution of fiber reinforcement to a composite material can be quantified as the intrinsic resistance of the fiber (σ_t^F) multiplied by its volume fraction in the composite (V^F). However, the effectiveness of the fiber is also constrained by the coupling or interface factor (f_c), which denotes the bonding between the fiber and matrix and is typically less than 1.[62] The contribution of the matrix to the composite's strength is represented by the

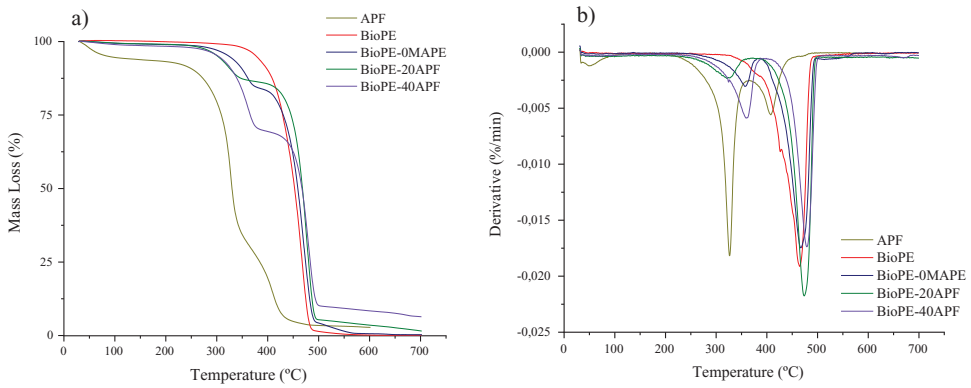

Figure 4. Results derived from the a) TGA and b) dTGA for the selected composites.

second term of the equation. It considers the matrix's strength at the point of deformation at break ($\sigma_t^{m^*}$), as obtained from a graph in **Figure 6**, and its volume fraction ($1 - V^F$). By considering both the contributions of the fiber and matrix, we can estimate the overall strength of the composite.

By assessing the rupture strain of the composites at 10%, 20%, 30%, and 40%, and subsequently plotting these values on a stress–strain graph for bio-polyethylene using a fifth-degree polynomial equation, we can ascertain the strength contributed by the matrix to each composite ($\sigma_t^{m^*}$), as detailed in **Table 4**.

However, the modified rule of mixtures equation introduces two variables that remain unknown: the coupling factor and the intrinsic strength of the fiber. Unfortunately, these variables cannot be determined experimentally. To address this challenge, three different assumptions were proposed, as summarized in Table 4.

Initially, the modified rule of mixtures equation (Equation 3) was solved with an assumed intrinsic fiber strength of 500 MPa. This value aligns with similar findings documented in the literature for fibers such as Barley, among others.[63,64] As anticipated, the tensile strength of the composite with 10% avocado decreased, resulting in a negative coupling factor. This implies that percentages below 20% should not be considered for evaluating avocado fibers due to poor interface properties. Conversely, when examining the results at 20%, 30%, and 40%, coupling factors of 0.1, 0.14, and 0.13 were observed, respectively. These average coupling factors of ≈0.12 notably fall below the optimal values reported in the literature (with f_c values ≈0.2).[65]

The second assumption taken into account was based on the consideration of a strong interface, assuming a coupling factor of 0.2. After, Equation 3 was used to determine the intrinsic strength of the fibers. Once again, in the case of the composite with 10% avocado, the weak fiber–matrix interface led to an unattainable value for the intrinsic strength of the fiber, as a fiber cannot possess negative strength. When examining other compounds under study, we observed that assuming a strong interface, the intrinsic strength of the avocado fibers would be 317 MPa. Although this value is relatively low, it does not deviate significantly from reported values for fibers like Barley.[63]

Finally, assuming an intrinsic strength of 500 MPa for the fibers and a strong interface with a coupling factor of 0.2, we determined the expected tensile strength of the composites. For the 10% avocado composite, the tensile strength should be almost 50% higher, while for the other compounds, it ranges between

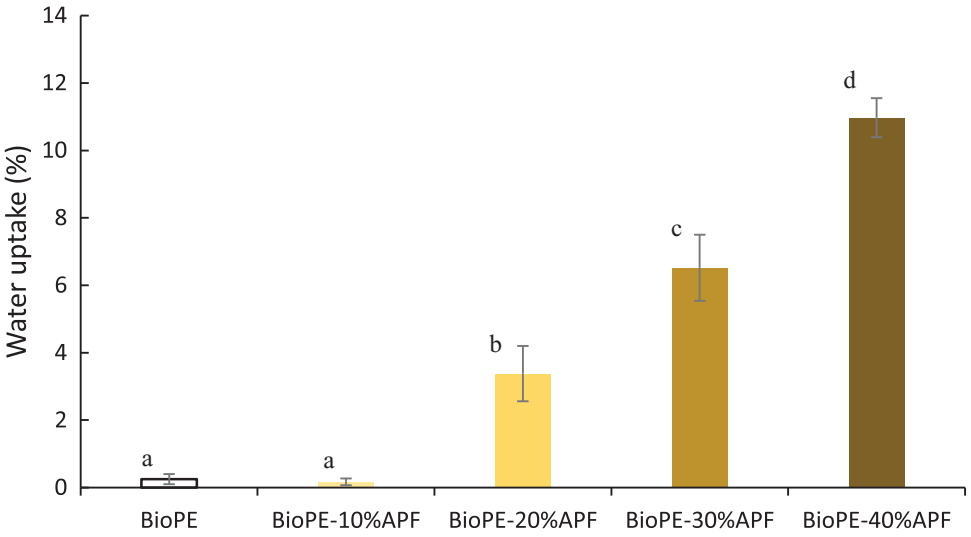

Figure 5. Results derived from the water uptake of the different biocomposites at time 24 h.

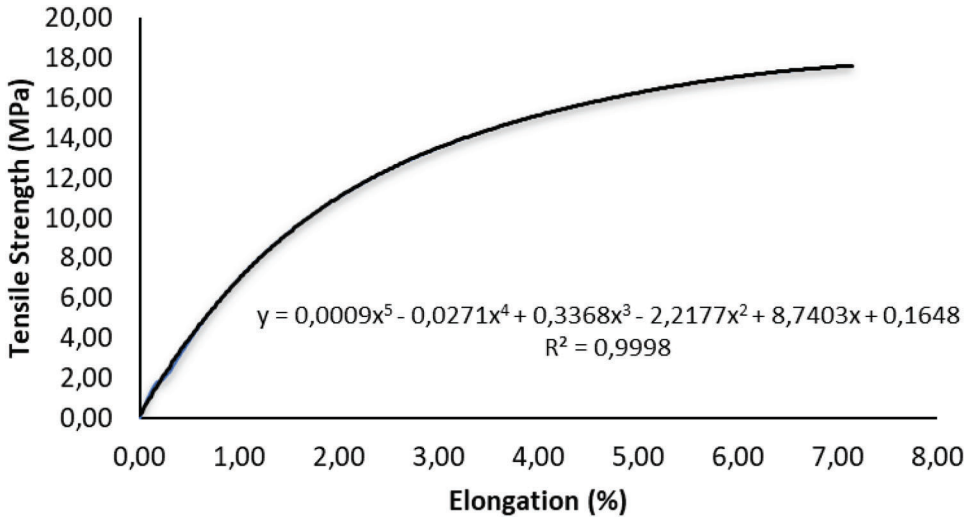

Figure 6. Tensile strength versus elongation curve of bio-polyethylene matrix.

20% and 30%. It is noteworthy that the composite with 30% avocado closely approximates the theoretically assumed tensile strength. This suggests that this percentage possesses physical characteristics such as flowability and fiber morphology that are close to the optimum. It is well-known that compounding and injection processes can significantly alter fiber morphology. When examining **Figure 7**, we can observe variations in the distribution of fiber lengths across different composites.

Subsequently, we applied the mathematical model of the modified Kelly–Tyson equation (Equation 4) using the Bowyer–Bader solution to calculate the intrinsic strength of avocado fibers.[66,67] this involved considering the fiber distribution depicted in Figure 7 and the stress–strain curves of the composites.

Table 4. Results of the simulated tensile strength calculated for each of the hypothesis raised.

Hypothesis 1					
Reinforcement Weight Content [%]	σ_t^C	$\sigma_t^{m^*}$	V^F	σ_t^F	f_c
10	16.28	19.03	0.066	500	-0.05
20	22.89	18.31	0.137	500	0.10
30	29.31	17.65	0.214	500	0.14
40	31.23	16.19	0.298	500	0.13
Average					0.12
Hypothesis 2					
Reinforcement Weight Content [%]	σ_t^C	$\sigma_t^{m^*}$	V^F	σ_t^F	f_c
10	16.28	19.03	0.066	-113	0.20
20	22.89	18.31	0.137	258	0.20
30	29.31	17.65	0.214	360	0.20
40	31.23	16.19	0.298	333	0.20
Average				317	
Hypothesis 3					
Reinforcement Weight Content [%]	σ_t^C	$\sigma_t^{m^*}$	V^F	σ_t^F	f_c
10	24.38	19.03	0.066	500	0.20
20	29.53	18.31	0.137	500	0.20
30	35.30	17.65	0.214	500	0.20
40	41.16	16.19	0.298	500	0.20

$$\sigma_t^C = \chi_1 \times \left(\sum_{L_c}^{i=0} \left[\frac{\tau \times l_i^F \times V_i^F}{d^F} \right] + \sum_{\infty}^{j=L_c} \left[\sigma_t^F \times V^F \times \left(1 - \frac{\sigma_t^F \times d^F}{4 \times \tau \times l_j^F} \right) \right] \right) + \left(1 - V^F\right) \times \sigma_t^{m^*} \quad (4)$$

In this case, we once again encounter the term representing the matrix contribution ($(1 - V^F) \times \sigma_t^{m^*}$), but we divide the fiber's contribution into two distinct factors. The first factor pertains to subcritical fibers, where the intrinsic strength of the fiber does not come into play. The second factor is applicable to supercritical fibers, where we multiply by the intrinsic strength of the fibers. This division between subcritical and supercritical fibers is governed by the critical length value (L_c), which represents the minimum fiber length required for the aspect ratio () to be adequate for the fibers to serve as reinforcement. The Kelly–Tyson equation also incorporates terms for interfacial shear strength (τ) and the orientation factor (χ_1).

It is well-established that the value of interfacial shear strength should closely align with the von Mises criterion ($\tau = \sigma_t^m/\sqrt{3}$) and the Tresca criterion ($\tau = \sigma_t^m/2$), which, in this context, are 10.4 and 9.2, respectively. Furthermore, the values of the orientation factor should be ≈0.31. With the result of τ, it becomes possible to calculate the critical length of the fibers as $L_c = (d^F \times \sigma_t^c)/2 \times \tau$.[68] The obtained results (**Table 5**) revealed that Bowyer–Bader yields an inaccurate solution for the 30% and 40% compositions. This discrepancy is likely attributed to minor deviations in the shape of the stress-strain curve, which exert a significant impact on the outcome.

Maintaining the χ_1 and τ values for the 20% composition, we proceeded to solve the Kelly–Tyson equation (Equation 4) to ascertain the intrinsic strength of avocado fibers, in addition to calculating the critical length, orientation factor, and interfacial shear strength (as presented in **Table 6**).

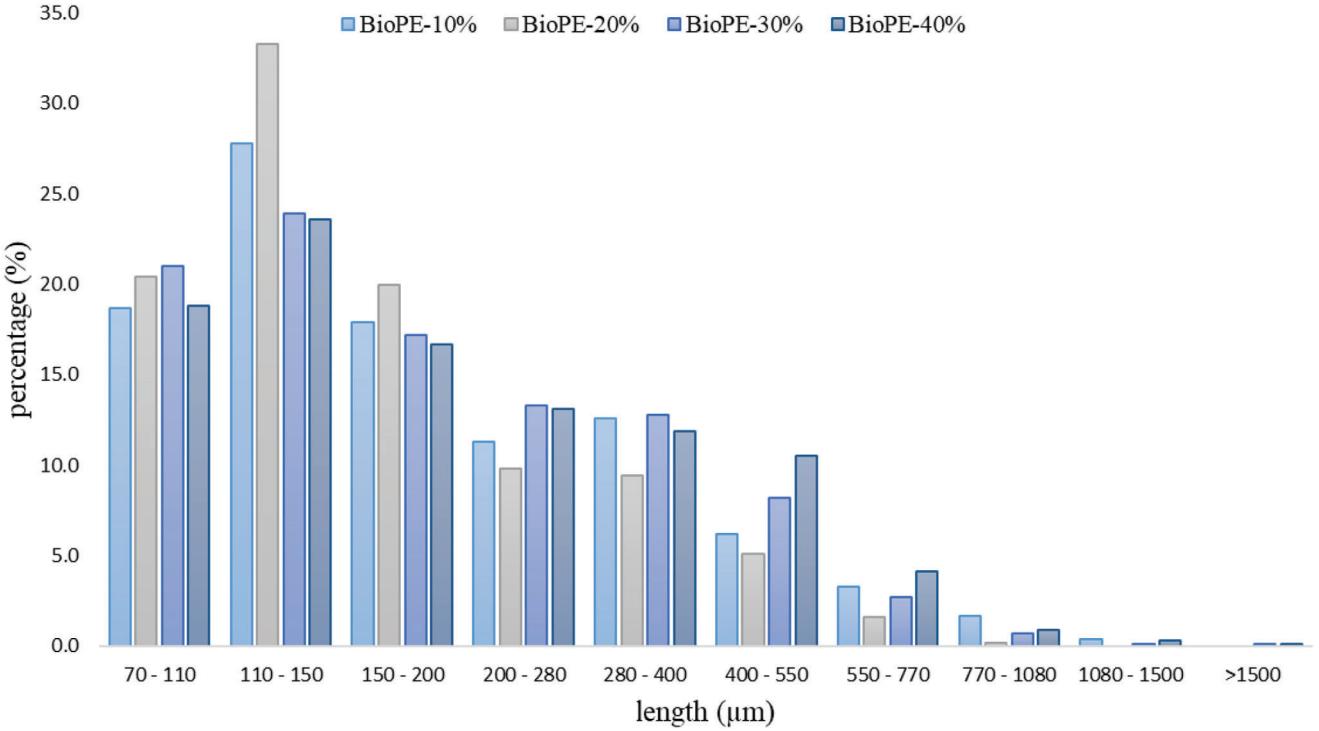

Figure 7. Fiber length distribution obtained after evaluating the APF extracted from the different composites.

Once this approximation is applied, it becomes evident that the intrinsic strength values of avocado fibers fall within the range of 364 and 515 MPa. These values closely align with those assumed in the initial approach for the modified rule of mixtures (as shown in **Table 7**). In this context, when constructing the coupling factor as the product of the orientation factor (χ_1) and the length and interface factor (χ_2), it is apparent that the coupling factor is optimal for the 30% reinforcement, while it decreases for the 20% and 40% compositions. Additionally, the average angle of the fibers (α) is a characteristic intrinsic to the injection machine and molds used, and it serves to validate the obtained results.

Based on the obtained results, we can represent the contribution of matrix strength (z), subcritical fibers (X), and supercritical fibers (Y) for the different composites (as shown in **Figure 8**). Notably, in the case of 40% composition, the higher presence of subcritical fibers results in an increased contribution from this fraction.

In contrast to the tensile strength of a composite material, Young's modulus remains unaffected by the interface.[69] Nonetheless, when we examine the modified rule of mixtures for Young's modulus (as defined in Equation 5), it becomes evident that a factor denoted as η_e emerges. This factor is essentially the

Table 5. Parameters used to solve the Kelly and Tyson equation by using the method proposed by Bowyer and Bader.

Reinforcement Weight Content [%]	20%	30%	40%
La	265.37	481.53	375.85
Ll	372.40	939.87	589.10
Lw	522.24	1625.87	914.82
Average length [µm]	189.14	246.69	239.86
Weighted average length [µm]	265.43	481.49	375.94
Weighted average length [µm]	372.23	832.93	583.81
Average diameter [µm]	21.30	22.40	24.90
σ_t^{m*}	18.31	17.65	16.19
χ_1	0.313	0.204	0.286
T	10.23	9.88	10.05
Lc	448.98	1052.81	1395.94
σ_t^F	431.21	928.34	1126.90

Table 6. Parameters used to solve the Kelly and Tyson equation by using the method proposed by Bowyer and Bader preserving the χ_1 and τ solution for the 20% biocomposite.

Reinforcement Weight Content [%]	20%	30%	40%
La	265.37	481.53	375.85
Ll	372.40	939.87	589.10
Lw	522.24	1625.87	914.82
Average length (µm)	189.14	246.69	239.86
Weighted average length (µm)	265.43	481.49	375.94
Weighted average length (µm)	372.23	832.93	583.81
Average diameter (µm)	21.30	22.40	24.90
σ_t^{m*}	18.31	17.65	16.19
χ_1	0.313	0.313	0.313
T	10.23	10.23	10.23
Lc	448.98	399.25	625.77
σ_t^F	431.21	364.67	514.19

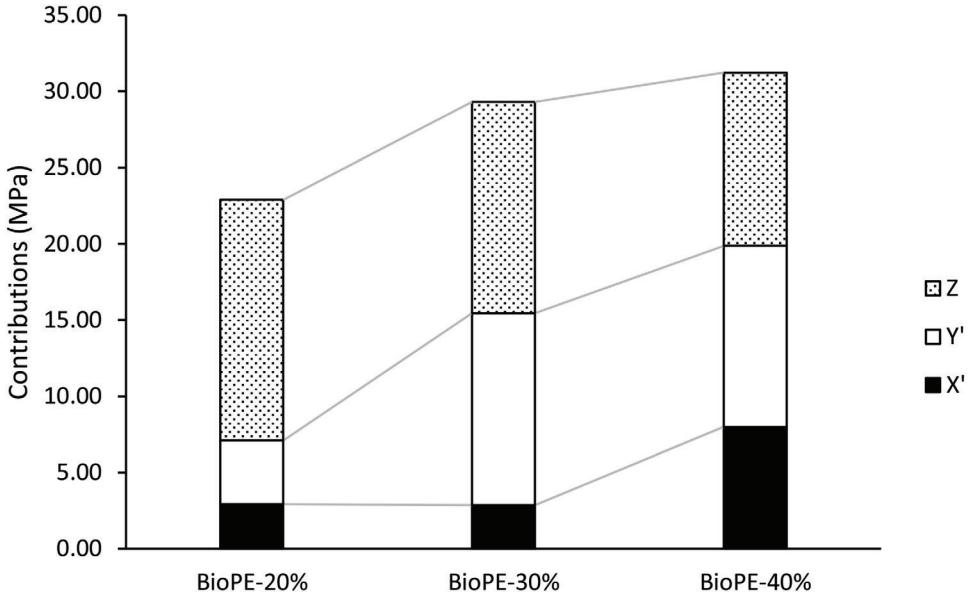

Figure 8. Contributions of the matrix, the subcritical, and the supercritical fibers to the tensile strength of the composites.

product of the length factor (η_l) and the orientation factor (η_o) for the modulus.

$$E_t^C = \eta_e \times E_t^F \times V^F + \left(1 - V^F\right) \times E_t^m \tag{5}$$

where E_t^F represents the intrinsic Young's modulus of the fibers, and E_t^m represents the modulus of the matrix.

Similarly, to the tensile strength, Equation 5 presents two unknowns and cannot be directly solved, in this case E_t^F and η_e. Once again, three assumptions were established (**Table 8**). In the first assumption, the intrinsic modulus of Barley fibers (16 GPa) was taken as the reference value. Solving Equation 5 revealed that the orientation and length factors were excessively high in comparison to reported values in the literature. As a result, in the second assumption, we established a factor value of 0.49. which is a typical value for natural fiber composites.[70,71] Solving Equation 4 led to significantly higher values for the intrinsic modulus of the fibers, close to 32 GPa. These values position the intrinsic modulus of avocado fibers within the range of fibers like abaca and those found in other plants.[69]

Finally, assuming a Young's modulus of 16 GPa for the fibers and a factor of 0.49, we can verify that the Young's modulus of the composite would have been notably lower. This suggests that the intrinsic modulus is higher, thereby leading to a more pronounced stiffening effect induced by the fibers.

Table 7. Results of the coupling factor (*fc*), orientation factor (χ_1), interface factor (χ_2), and angle of the fibers (α) for the different biocomposites.

Reinforcement Weight Content [%]	20%	30%	40%
Fc	0.12	0.20	0.13
χ_1	0.31	0.31	0.31
χ_2	0.38	0.63	0.41
A	60.64	60.64	60.64

To further affirm the intrinsic modulus of the fibers and assess its comparability with the value from assumption 2 (31.53 GPa), we explored a solution using the Hirsch model (as defined in Equation 6)[72]:

$$E_t^C = \beta \times \left(E_t^F \times V^F + \left(1 - V^F\right) \times E_t^m\right) + (1 - \beta) \times \frac{E_t^F \times E_t^m}{E_t^m \times V^F + E_t^f \times (1 - V^F)} \tag{6}$$

Table 8. Results of the simulated Young´s modulus calculated for each of the hypothesis raised.

Hypothesis 1					
Reinforcement Weight Content [%]	E_t^C	E_t^m	V^F	E_t^F	η_e
10	2.18	1.06	0.07	16	1.13
20	2.92	1.06	0.14	16	0.91
30	4.12	1.06	0.21	16	0.96
40	4.87	1.06	0.3	16	0.87
Average					0.97
Hypothesis 2					
Reinforcement Weight Content [%]	E_t^C	E_t^m	V^F	E_t^F	η_e
10	2.18	1.06	0.07	36.8	0.49
20	2.92	1.06	0.14	29.8	0.49
30	4.12	1.06	0.21	31.3	0.49
40	4.87	1.06	0.3	28.3	0.49
Average				31.5	
Hypothesis 3					
Reinforcement Weight Content [%]	E_t^C	E_t^m	V^F	E_t^F	η_e
10	1.51	1.06	0.07	16	0.49
20	1.99	1.06	0.14	16	0.49
30	2.51	1.06	0.21	16	0.49
40	3.08	1.06	0.3	16	0.49

Table 9. Solutions obtained for Equation 4 for the different biocomposites.

Reinforcement Weight Content (%)	20%	30%	40%
E_t^F Hirsch	33.15	34.80	30.87
η_e	0.44	0.44	0.45
η_l	0.81	0.90	0.90
η_o	0.55	0.49	0.50

where β is the stress transfer factor by fiber and matrix, typically 0.4 in short fiber semi-aligned composites.

The solution to Equation 5 for the composites with 20%, 30%, and 40% reported intrinsic modulus values of the fibers that closely matched those assumed in hypothesis 2 (as detailed in **Table 9**). At the same time, it was confirmed that the orientation and length factor was 0.44, which is very close to the expected value of 0.49. This is because the length factor was ≈0.87 and the orientation factor was 0.51.

The micromechanical results allowed us to determine that the intrinsic strength of avocado fibers is ≈437 MPa, and their intrinsic modulus is ≈33 GPa. These values are far from the properties of fibers like Hemp, which have an intrinsic strength of over 800 MPa.[73] Additionally, we found that the 30% composition exhibited a stronger interface. Therefore, while avocado fibers can reinforce the bio polyethylene matrix, they do not lead to significant increases in tensile strength. However, they do contribute to a significant increase in the Young's modulus of the composite. Despite these differences in the performance of the fibers, it's important to highlight that while Hemp, jute or bamboo are known for their favorable properties and eco-friendly characteristics, they often require dedicated cultivation and harvesting processes. In contrast, in this study a lignocellulosic residue is used, and their characteristics differ greatly from other raw materials used for fiber-reinforced biocomposites. However, the use of APW for the development of biocomposites has proven to be useful. With the aim of further characterize the materials, additional analyses were conducted to examine the morphology and thermal stability of the samples.

4. Conclusion

This study showcases the potential of avocado pruning residues as a renewable resource for partially replacing non-biodegradable plastic polymers in food packaging, specifically biobased polyethylene. The incorporation of maleated polyethylene (MAPE) as a fiber–polymer compatibilizer significantly enhances the mechanical properties of the composites. The addition of 9% w/fw MAPE (based on the fiber) resulted in a significant 25.5% increase in tensile strength compared to uncoupled composites, indicating stronger bonding between the fiber and polymeric matrix, as observed in SEM micrographs. However, higher concentrations of MAPE led to an increase in short-chain polyethylene, negatively impacting the composite interface. Despite the evidence of the effectiveness of MAPE, it would be interesting to carry out complementary analyses, such as FTIR, to check for the presence of covalent ester bonds at the interface. Furthermore, incorporating APF at concentrations equal to or higher than 20% (w/w) was able to reinforce the polymeric matrix increasing the tensile strength and Young's modulus by 49% and 325% in BioPE-40APF composites, respectively. In terms of intrinsic properties, the micromechanical study revealed that the intrinsic strength of avocado fibers is ≈437 MPa, and their intrinsic modulus is ≈33 GPa, with BioPE-30APF biocomposite exhibiting the stronger interface. While this research provides the optimization and preliminary characterization the APW-derived materials for their application in the food packaging industry, further investigations are necessary. Specifically, additional characterization is required to evaluate essential properties for food packages, such as migration, solubility, and water retention capacity. Additionally, conducting economic and life cycle studies would be beneficial to assess the overall profitability and sustainability of the process.

Supporting Information

Supporting Information is available from the Wiley Online Library or from the author.

Acknowledgements

The authors acknowledge the financial support from the Ministerio de Ciencia e Innovación (MCINN) of Spain in the form of a national project, PID2020-117718RB-I00, as part of the national programme of R+D projects «Retos Investigación» y «Generación de Conocimiento», funded by MCIN/AEI/10.13039/501100011033 and to the Consejería de Universidad, Investigación e Innovación of Andalusian Regional Government for the support and funding thanks to the pre-doctoral contracting of research personnel in training by the agents of the Andalusian knowledge system (code 24653). The authors also thank the staff of the Central Research Support Service (SCAI) of the University of Córdoba. Marc Delgado-Aguilar and Quim Tarrés are Serra Huter fellows.

Conflict of Interest

The authors declare no conflict of interest.

Data Availability Statement

The data that support the findings of this study are available from the corresponding author upon reasonable request.

Keywords

avocado residue, biobased packaging, biocomposites, injection molding, material modellng

Received: November 25, 2023
Revised: February 16, 2024
Published online: March 15, 2024

[1] K. Marsh, B. Bugusu, *J. Food Sci.* **2007**, *72*, R39.
[2] The New Plastic Economy: Rethinking the Future of Plastics, https://www.ellenmacarthurfoundation.org/the-new-plastics-economy-rethinking-the-future-of-plastics (accessed: October 2023).

[3] Global plastic production from 1950 to 2021, https://es.statista.com/estadisticas/636183/produccion-mundial-de-plastico/ (accessed: October 2023).
[4] R. Geyer, J. R. Jambeck, K. L. Law, *Sci. Adv.* **2017**, *3*, 1700782.
[5] G. Fredi, A. Dorigato, *Adv. Ind. Eng. Polym. Res.* **2021**, *3*, 159.
[6] I. Wojnowska-Baryła, D. Kulikowska, K. Bernat, *Sustain* **2020**, *12*, 2088.
[7] Directive (EU) 2019/904 of the European Parliament and of the Council of 5 June 2019 on the reduction of the impact of certain plastic products on the environment, https://eur-lex.europa.eu/eli/dir/2019/904/oj (accessed: October 2023).
[8] Directive (EU) 2018/852 of the European Parliament and of the Council of 30 May 2018 amending Directive 94/62/EC on packaging and packaging waste, https://eur-lex.europa.eu/eli/dir/2018/852/oj (accessed: October 2023).
[9] Questions and Answers – Communication on a policy framework for biobased biodegradable and compostable plastics, https://ec.europa.eu/commission/presscorner/detail/en/qanda_22_7158 (accessed: October 2023).
[10] M. Kan, S. A. Miller, *Resour. Conserv. Recycl.* **2022**, *180*, 106156.
[11] Á. J. Aguirre, G. E. Guevara-Viera, C. S. Torres-Inga, R. V. Guevara-Viera, A. Boné, M. Vidal, F. J. García-Ramos, *Appl. Sci.* **2020**, *10*, 5029.
[12] K. E. Semple, C. Zhou, O. J. Rojas, W. N. Nkeuwa, C. Dai, *Food Packag. Shelf Life* **2020**, *33*, 100908.
[13] C. Zarna, M. T. Opedal, A. T. Echtermeyer, G. Chinga-Carrasco, *Compos. Part C Open Access.* **2021**, *6*, 100171.
[14] Areas and annual crop production, https://www.mapa.gob.es/es/estadistica/temas/estadisticas-agrarias/agricultura/superficies-producciones-anuales-cultivos/ (accessed: October 2023).
[15] Areas and annual crop production, https://www.mapa.gob.es/es/estadistica/temas/estadisticas-agrarias/agricultura/superficies-producciones-anuales-cultivos/ (accessed: January 2024).
[16] S. Paniagua, S. Reyes, F. Lima, N. Pilipenko, L. F. Calvo, *Fuel.* **2021**, *291*, 119660.
[17] R. Vargas, J. R. Sanjuán D, J. A. Silva G, J. Rivera P, F. J. Fuentes T, H. G. Richter, *Madera y Bosques* **2006**, *12*, 1211248.
[18] E. Espinosa, F. Rol, J. Bras, A. Rodríguez, *J. Clean. Prod.* **2019**, *239*, 118083.
[19] Q. Tarrés, M. Ardanuy, *Polymers* **2020**, *12*, 1308.
[20] Y. Lei, Q. Wu, C. M. Clemons, F. Yao, Y. Xu, *J. Appl. Polym. Sci.* **2007**, *106*, 3958.
[21] A. M. Noor Azammi, R. A. Ilyas, S. M. Sapuan, R. Ibrahim, M. S. N. Atikah, M. Asrofi, A. Atiqah, *Interfaces in Particle and Fibre Reinforced Composites*, Elsevier, Amsterdam, The Netherlands **2020**.
[22] J. A. Dávila, M. Rosenberg, E. Castro, C. A. Cardona, *Bioresour. Technol.* **2017**, *243*, 17.
[23] M. M. Kabir, H. Wang, K. T. Lau, F. Cardona, *Compos. Part B Eng.* **2102**, *43*, 2883.
[24] J. Yang, Y. C. Ching, C. H. Chuah, *Polymers* **2019**, *11*, 751.
[25] M. M. Kabir, H. Wang, K. T. Lau, F. Cardona, *Compos. Part B Eng.* **2012**, *43*, 2883.
[26] S. S. Nair, H. Chen, Y. Peng, Y. Huang, N. Yan, *ACS Sustainable Chem. Eng.* **2018**, *6*, 10058.
[27] Z. H. Zhu, B. H. Mo, M. Y. Hao, *IOP Conf. Ser. Mater. Sci. Eng.* **2019**, *544*, 012012.
[28] I. Elfaleh, F. Abbassi, M. Habibi, F. Ahmad, M. Guedri, M. Nasri, C. Garnier, *Results Eng.* **2023**, *19*, 101271.
[29] J. Chen, Y. Wang, C. Gu, J. Liu, Y. Liu, M. Li, Y. Lu, *Materials* **2013**, *6*, 2483.
[30] Y. Wang, *IOP Conf. Ser. Earth Environ. Sci.* **2021**, *726*, 012005.
[31] T. J. Keener, R. K. Stuart, T. K. Brown, *Compos. Part A Appl. Sci. Manuf.* **2004**, *35*, 357.
[32] J. Z. Lu, Q. Wu, I. I. Negulescu, *Wood Fiber Sci.* **2002**, 34.
[33] Y. Wang, D. Ji, C. Yang, H. Zhang, C. Qin, B. Huang, *J. Appl. Polym. Sci.* **1994**, *52*, 1411.
[34] F. Seculi, F. Julián, J. Llorens, F. X. Espinach, P. Mutjé, Q. Tarrés, *Polymers (Basel)* **2023**, *15*, 3137.
[35] A. M. Jiménez, M. Delgado-Aguilar, Q. Tarrés, G. Quintana, P. Fullana-i-Palmer, P. Mutjè, F. X. Espinach, *BioResources* **2017**, *12*, 3618.
[36] L. A. Granda, F. X. Espinach, J. A. Méndez, J. Tresserras, M. Delgado-Aguilar, P. Mutjé, *Compos. Part B Eng.* **2016**, *92*, 332.
[37] M. E. Vallejos, F. X. Espinach, F. Julián, L. Torres, F. Vilaseca, P. Mutjé, *Compos. Sci. Technol.* **2012**, *72*, 1209.
[38] E. F. Santos, R. S. Mauler, S. M. B. Nachtigall, *J. Reinf. Plast. Compos.* **2009**, *28*, 2119.
[39] B. Chihaoui, F. Serra-Parareda, Q. Tarrés, F. X. Espinach, S. Boufi, M. Delgado-Aguilar, *Polymers* **2020**, *12*, 1693.
[40] S. Mohanty, S. K. Verma, S. K. Nayak, *Compos. Sci. Technol.* **2006**, *66*, 538.
[41] A. Carbonell-Verdú, D. García-García, A. Jordá, M. D. Samper, R. Balart, *Compos. Part B Eng* **2015**, *69*, 460.
[42] F. X. Espinach, E. Espinosa, R. Reixach, A. Rodríguez, P. Mutjé, Q. Tarrés, *Polymers* **2020**, *12*, 2206.
[43] E. K. Gamstedt, R. Sandell, F. Berthold, T. Pettersson, N. Nordgren, *Mech. Mater.* **2011**, *43*, 693.
[44] E. Tarani, I. Arvanitidis, D. Christofilos, D. N. Bikiaris, K. Chrissafis, G. Vourlias, *J. Mater. Sci.* **2023**, *58*, 1621.
[45] S. Mohanty, S. K. Nayak, *J. Reinf. Plast. Compos.* **2010**, *29*, 2199.
[46] F. S. da Silva, C. B. B. Luna, D. D. Siqueira, E. da Silva Barbosa Ferreira, E. M. Araújo, *J. Polym. Environ.* **2022**, *30*, 1028.
[47] A. Fendler, M. P. Villanueva, E. Gimenez, J. M. Lagarón, *Cellulose* **2007**, *14*, 427.
[48] J. Chen, N. Yan, *Compos. Part B Eng.* **2013**, *54*, 180.
[49] A. Khouaja, A. Koubaa, H. B. Daly, *Ind. Crops Prod.* **2011**, *171*, 113928.
[50] A. Makhlouf, A. Belaadi, S. Amroune, M. Bourchak, H. Satha, *J. Nat. Fibers.* **2022**, *19*, 3928.
[51] J. R. Araújo, W. R. Waldman, M. A. De Paoli, *Polym. Degrad. Stab.* **2008**, *93*, 1770.
[52] B. Rashid, Z. Leman, M. Jawaid, M. J. Ghazali, M. R. Ishak, *Cellulose* **2016**, *23*, 2905.
[53] M. J. Ahmed, M. S. Balaji, S. S. Saravanakumar, M. R. Sanjay, P. Senthamaraikannan, *J. Ind. Text.* **2019**, *49*, 294.
[54] B. Tajeddin, L. C. Abdulah, *Polym. Polym. Compos.* **2010**, *18*, 257.
[55] D. R. Mulinari, H. J. C. Voorwald, M. O. H. Cioffi, M. L. C. P. da Silva, *J. Compos. Mater.* **2017**, *51*, 1807.
[56] H. Awais, Y. Nawab, A. Amjad, A. Anjang, H. M.d Akil, M. S. Zainol Abidin, *Compos. Part C Open Access.* **2021**, *4*, 100082.
[57] H. Alamri, I. M. Low, *Polym. Test.* **2012**, *31*, 620.
[58] M. Berthet, H. Angellier-coussy, D. Machado, L. Hilliou, A. Staebler, A. Vicente, N. Gontard, *Ind. Crops Prod.* **2015**, *69*, 110.
[59] E. L. Sánchez-safont, A. Aldureid, J. María, J. Gámez-pérez, L. Cabedo, *Compos. Part B.* **2018**, *145*, 215.
[60] H. Fukuda, T. W. Chou, *J. Mater. Sci.* **1982**, *17*, 1003.
[61] Y. G. Korabel´nikov, I. A. Rashkovan, *Fibre Chem.* **2006**, *38*, 142.
[62] A. R. Sanadi, R. A. Young, C. Clemons, R. M. Rowell, *J. Reinf. Plast. Compos.* **1994**, *13*, 54.
[63] F. Serra-Parareda, Q. Tarrés, M. Delgado-Aguilar, F. X. Espinach, P. Mutjé, F. Vilaseca, *Materials* **2019**, *12*, 4182.
[64] M. Hyvärinen, T. Kärki, *MATEC WebConf.* **2015**, *30*, 01014.
[65] M. Rodriguez, A. Rodriguez, R. J. B., F. Vilaseca, J. Girones, P. Mutje, *BioResources* **2010**, *5*, 2535.
[66] A. Kelly, W. R. Tyson, *J. Mech. Phys. Solids.* **1965**, *13*, 329.
[67] W. H. Bowyer, M. G. Bader, *J. Mater. Sci.* **1972**, *7*, 1315.

[68] Y. Li, K. L. Pickering, R. L. Farrell, *Compos. Sci. Technol.* **2009**, *69*, 1165.
[69] F. Serra-Parareda, F. Vilaseca, F. X. Espinach, P. Mutjé, M. Delgado-Aguilar, Q. Tarrés, *Polymers* **2021**, *13*, 619.
[70] G. Kalaprasad, K. Joseph, S. Thomas, C. Pavithran, *J. Mater. Sci.* **1997**, *32*, 4261.
[71] R. Reixach, F. X. Espinach, E. Franco-Marquès, F. Ramirez De Cartagena, N. Pellicer, J. Tresserras, P. Mutjé, *Polym. Compos.* **2013**, *34*, 1840.
[72] T. J. Hirsch, *J. Proc.* **1962**, *59*, 427.
[73] R. J. Aguado, F. X. Espinach, F. Julián, Q. Tarrés, M. Delgado-Aguilar, P. Mutjé, *Polymers* **2023**, *15*, 146.

